Tailoring the linear viscoelastic response of industrial double dynamics networks through the interplay of associations

Consiglia Carillo, Stephan Zoellner, Evelyne van Ruymbeke, et al.

Citation: Journal of Rheology **66**, 1239 (2022); doi: 10.1122/8.0000406
View online: https://doi.org/10.1122/8.0000406
View Table of Contents: https://sor.scitation.org/toc/jor/66/6
Published by the The Society of Rheology

Tailoring the linear viscoelastic response of industrial double dynamics networks through the interplay of associations

Consiglia Carillo,[1,2] Stephan Zoellner,[3] Evelyne van Ruymbeke,[4] and Dimitris Vlassopoulos[1,2,a)]

[1]*FORTH, Institute of Electronic Structure and Laser, Heraklion 70013, Crete, Greece*
[2]*Department of Materials Science and Technology, University of Crete, Heraklion 70013, Crete, Greece*
[3]*TESA SE, 22848 Norderstedt, Germany*
[4]*Institute of Condensed Matter and Nanosciences (IMCN), Université catholique de Louvain, Bio and Soft Matter Division (BSMA), Louvain-la-Neuve, Belgium*

(Received 29 November 2021; final revision received 13 January 2022; published 1 November 2022)

Abstract

We investigate the linear viscoelastic properties of industrial pressure sensitive adhesives comprising double networks with an entangled acrylate-based polymer and two types of intermolecular associations (crosslinking), permanent (epoxide) and reversible (metal-chelate), having different compositions. A combination of shear rheometry and an appropriately modified version of the Time Marching Algorithm (TMA) allows to probe and analyze the behavior of the different double dynamic networks, in particular, the effects of the type and amount of crosslinks on their linear viscoelastic spectra. To this end, the dynamics of the double networks are compared with the respective individual responses of the polymeric component without crosslinks and the single networks (possessing only physical or only chemical crosslinks), in order to quantify their contributions to the relaxation mechanisms, particularly the interplay between disentanglement and bond association/dissociation processes. With the help of the TMA model, we also examine the respective roles of the lifetime of stickers, polydispersity, and molar mass. Triggered by the good comparison between predictions and experimental data, we propose a framework to tune material parameters in order to obtain a desired viscoelastic behavior. © *2022 The Society of Rheology.* https://doi.org/10.1122/8.0000406

I. INTRODUCTION

Pressure sensitive adhesives (hereafter PSAs) represent a class of commodity polymeric materials able to stick to a variety of surfaces upon contact and to detach without leaving any residues. They differ from other adhesives for their ability to bond to the surface when a light pressure (finger pressure) is applied, without any chemical reaction [1–3]. PSAs have been widely used since the 19th century in different fields, including everyday products. Their application ranges from labeling and packaging to the assembly of automotive parts, toys, and electronic circuits, with also a strong impact on pharmaceutical products or processes, like medical tapes, dressings, transdermal drug delivery, and other skin applications that require flexibility, compatibility with the skin, and moisture permeability [4–8].

Adhesive properties are highly influenced by the viscoelastic nature of the materials: the viscous response ensures the ability to flow and dissipate energy during the bonding process, i.e., the adhesion to surfaces, while the elastic response provides good peel performance and guarantees resistance to creep, avoiding failure during detachment [2]. Consequently, optimizing and tailoring the properties of PSAs mandates understanding the interplay of their viscoelastic behavior with their adhesive characteristics [9–11]. The ability to wet a surface and create bonds is linked to the softness of the PSAs. In particular, the Dahlquist criterion suggests that a good contact is ensured for values of the storage modulus G' below 3×10^5 Pa, when a deformation is applied for 1 s [12]. When the application requires tack with different deformation times, higher stiffness is required for longer dwell times and lower G' for shorter times or rough surfaces [13]. On the other hand, relatively high and broadly distributed (in time) values of the loss modulus G'' are needed to ensure energy dissipation, yielding good resistance to deformation and good peel properties. The latter is also associated with strain hardening to ensure the absence of sticky residues following peeling from a surface [14]. Therefore, it is evident that PSA formulations need the right balance between adhesive and cohesive properties in order to perform in response to set specifications. Understanding how to control this balance, which directly depends on their viscoelastic behavior and, of course, their chemical composition, represents an outstanding challenge in the field. In general, PSAs are made of sparsely crosslinked polymer networks with a low glass transition temperature, but in the last few years, several efforts have been made to reach a balance between dissipative ability and resistance to flow and elastic response in order to meet the above challenge. The use of different topologies like bottlebrush polymers [15], rather than the usual linear or slightly branched polymers, and the introduction of supramolecular interactions [16–18], which are able to dissipate energy upon deformation, are promising approaches that have been used with

Note: This paper is part of the special issue on Double Dynamics Polymeric Networks

[a)]Author to whom correspondence should be addressed; electronic mail: dvlasso@iesl.forth.gr

some success, and so is the implementation of double or triple networks which incorporates sacrificial bonds into a secondary network [19,20]. Of special interest are double networks, which have attracted a great deal of attention in different fields due to their unique combination of mechanical strength and stretchability [21,22] and represent the thrust of the present work. In the case of PSAs, the chemical crosslinkers provide high mechanical strength and elasticity, whereas the physical network plays the role of sacrificial component, allows energy dissipation when detaching forces are applied [23,24], and contributes to high peel resistance. Hence, the use of two different types of bonds improves peel and shear resistance properties without altering the tack response as ensured by the low plateau modulus of the samples, according to the Dahlquist criteria.

Considering the relevance of the linear viscoelastic response to the adhesive properties of double networks, we aim to investigate the dynamics of industrial PSAs and compare with the constituent single networks, in order to quantify the influence of fundamental parameters such as the crosslinking density or the relative proportion of permanent component, lifetime of the bonds and molecular weight distribution on the rheological properties. Understanding how these parameters contribute to the viscoelastic response of the networks is indeed a key element to tailor the properties of the networks toward the design of PSAs with desired performance. To achieve our goal, we combine linear rheological experiments with modeling by means of a modified Time Marching Algorithm (TMA), which is able to capture the rheological features of nonideal networks characterized by a high polydispersity and a random distribution of crosslinks of varying density.

In Secs. II A–II C, we first introduce the materials used and chemical characteristics of the networks as well as the methods employed to study their dynamics. Subsequently, we present the experimental results and discuss the effects of the different crosslink compositions on the linear viscoelasticity of the double networks. A description of the model implementation and the predictions obtained for the different networks are presented next, along with the model validation and parametric analysis. Finally, we conclude by pointing on the role of the different model parameters on the rheological response of the PSAs.

II. MATERIALS AND METHODS

A. Materials

The double networks investigated are industrial acrylate-based PSAs synthesized by TESA SE (Hamburg, Germany). They are obtained from a highly polydisperse linear copolymer, weakly crosslinked with permanent and reversible bonds. The molecular characteristics are reported in Table I.

The dynamics of the Pristine sample (polymer without crosslinks) and the single networks (bonded by only physical or only chemical bonds) with different amounts of stickers were examined, in order to determine their influence on the rheological response of the double networks. In Table II, we list the samples investigated and the fraction of stickers. All were prepared and provided by TESA SE.

TABLE I. Molecular characteristics of the double network used.

Co-monomer composition	Butyl acrylate/2-ethylhexyl acrylate/acrylic acid 47.5:47.5:5 (by wt. %)
Reversible crosslinker	Aluminium acetylacetonate
Permanent crosslinker	Tetrakis(2,3-epoxylpropyl)-m-xylol-a,a'diamin
M_n(g/mol)	37 800 (number-average molar mass)
M_w(g/mol)	851 000 (weight-average molar mass)

TABLE II. Composition of network samples investigated.

Sample	Ionic stickers (wt. %) (reversible)	Covalent stickers (wt. %) (permanent)
Pristine	—	—
Double A	0.075	0.035
Double B	0.05	0.025
Reversible I	0.075	—
Reversible II	0.106	—
Permanent I	—	0.035
Permanent II	—	0.118

Samples Reversible I and Permanent I contain the same weight fraction of reversible and permanent crosslinkers, respectively, as sample Double A. On the other hand, samples Reversible II and Permanent II were prepared in order to have the same weight fraction of reversible and permanent crosslinkers, respectively, with the total concentration of bonds (i.e., including both reversible and permanent bonds) of sample Double A. Thus, the absolute number of connection points should be the same. Double B is characterized by different fractions of crosslinkers compared to Double A; there is no specific correspondence to the other single networks.

B. Experimental details

The linear viscoelastic properties of the networks were measured with a MCR 702 rheometer (Anton Paar, Austria), equipped with a CTD 180 hybrid oven, which provides a temperature control with a Peltier element and flow of nitrogen gas. The geometry used was a stainless steel parallel plate with a diameter of 8 mm. The samples were provided in the form of films of 0.1 mm thickness. In order to properly load the samples into the rheometer, we formed a single specimen of about 1 mm thickness by stacking the films on top of each other. The specimen was pressed under vacuum in order to remove possible bubbles and inhomogeneities and then shaped into discs of the needed radius by means of a punching tool.

After loading the samples and waiting for complete relaxation of the normal force, the samples were equilibrated at 100 °C for 2 h. Afterward, oscillatory measurements were performed in the linear viscoelastic regime, at temperatures ranging from 5 to 100 °C. The upper limit was set by the degradation occurring at higher temperatures (and confirmed by the time-evolving moduli). At each temperature, sample equilibration was monitored by means of a dynamic time sweep test ($\omega = 1$ rad/s, $\gamma = 5\%$), which probes the

evolution of G' and G'' for about 10 h. The linear viscoelastic regime was determined with the help of dynamic strain sweep tests ($\omega = 10$ rad/s, $\gamma = 0.1 - 500\%$), whereas dynamic frequency sweep (DFS) tests were performed (typically at strain amplitude $\gamma = 5\%$ in the linear regime) in order to investigate the dynamics of the networks in the frequency range 100–0.01 rad/s.

Given the upper limit in the temperature mentioned above, we performed creep measurements at 60 °C in the linear viscoelastic regime to extend the dynamic spectra to lower frequencies. The linear response was ensured for each sample by applying different stresses and verifying the overlap of the resulting creep compliance data. The latter were then converted into dynamic moduli using the NLREG software, based on the Tikhonov regularization method [25,26].

Master curves of frequency-dependent moduli (Fig. 2) were generated by applying the principle of time temperature superposition (TTS) at a reference temperature of 30 °C. To examine the master curves with better resolution and assess the thermorheological simplicity (or lack of it) of the tested samples, Van Gurp–Palmen (VGP) plots of phase angle versus complex modulus were constructed (see Fig. S1 in the supplementary material) [27,48]. We concluded that, despite some scattering in the VGP representations of the same samples, all networks were thermorheologically simple. As further discussed in Sec. III, this suggests that in the investigated temperature range the stickers do not significantly affect the thermorheological behavior of networks. The same horizontal shift factors were used for all samples (see Fig. S2 in the supplementary material [48]), whereas no vertical shifting was performed (the temperature dependence of the density for the different samples is not known) and this may explain slight imperfections in the master curves. The master curves were shifted to become iso-frictional, i.e., at the same distance from the glass transition temperature (T_g), which was determined by differential scanning calorimetry (using a DSC 250 instrument, from TA Instruments). During the DSC measurements, the samples were heated with a rate of 10 °C/min under constant nitrogen purge flow, from −100 to 80 °C.

C. Modeling analysis

1. Time marching algorithm

We have extended the TMA in order to describe the linear viscoelasticity of the present industrial double networks. The modeling of the parent material and the single networks was also performed, and the results contributed to the emerging picture of the dynamics of the double networks.

TMA has been extensively used to describe the viscoelastic properties of a variety of polymeric materials with different architectures [28–30] and physical (reversible) associations [31–34] and was proven to be a reliable predictive tool for their rheology. The model implements the known tube-based relaxation mechanisms [35–37], i.e., reptation, contour length fluctuations and constraint release (CR) modes (CR Rouse motion and dynamic tube dilation), while it accounts for the hierarchical relaxation in branched polymers using a specific molecular coordinate system [28]. Depending on the details of the macromolecular structure, the contribution of each relaxation mechanism to the overall dynamics may differ. More specifically, TMA describes and interconnects the relaxation processes involved, following the relaxation of a chain along a discretized time axis, and estimating the survival probabilities at a given time for a molecular segment to remain oriented (unrelaxed), from the corresponding values at the previous time step. The unrelaxed fraction of polymer chains, which contributes to the stress relaxation modulus $G(t)$, is described by a statistical approach that considers the probability for each segment to relax by a distinct mechanism [38]. This probability is updated at each time step in order to consider the effects of the relaxed segments, which dilute the constraints of the remaining (unrelaxed) segments. Consequently, $G(t)$ can be calculated at each time step and then the dynamic moduli (G' and G'') are obtained from the Schwarzl approximation [39],

$$G(t) = G_N^0 \, \Phi(t) + F_{LR}(t) + F_{FR}(t), \tag{1}$$

where $F_{LR}(t)$ and $F_{FR}(t)$ represent the contributions of the longitudinal and transverse Rouse modes [40], respectively, G_N^0 is the plateau modulus, and $\Phi(t)$ is the fraction of the tube at time t that has not yet relaxed. The latter is a function of the different probabilities for the modes of reptation, fluctuation, and CR processes (due to the environment of a relaxing chain segment), p_{rept}, p_{fluc}, and p_{envir}, respectively. Further details are given in [32].

2. Model implementation details

A Matlab code was developed to describe the statistical composition of a double polymeric network. The prediction of the linear viscoelastic response of the Pristine sample stems from the model described in [32] for linear chains. When bonds are introduced, $G(t)$ is estimated with a statistical approach that considers an additional parameter p representing the probability that a chain segment unit is associated (crosslinked), following a protocol similar to that of [26]. Once the probability p is fixed, the stickers are randomly added into the system and the model simulates the distribution of the different segments in the network (free linear chains, star-like chains containing only one associated unit, dangling ends, and trapped segments having two associated units at their ends).

Starting from a given molar mass distribution (MMD) (see Appendix, Fig. 14) of the polymeric chains before crosslinking (Pristine sample), a large ensemble of chains is generated and reversible or permanent crosslinkers are added in a statistical way (following Flory statistics), with respective probabilities p_1 and p_2. The chains are divided into monomeric units of molar mass 152 g/mol (estimated from chemistry) and are then analyzed to determine which monomeric unit is a crosslinking point. To do so, a value between 0 and 1 is randomly assigned to each of them and compared to the value of fixed probability p (p_1 or p_2). When the latter is higher than the random value, then the monomer is considered to be a crosslinking point.

The model considers 14% of the short polymer chains ($M_w \ll M_e$) acting as a solvent, as justified by the

experimental MMD of Fig. 14 of the Appendix. In addition, we need to define the three material parameters used in tube models, i.e., the entanglement plateau modulus, the average molar mass of a segment between two entanglements, and its Rouse time. These parameters, which do not depend on the sample architecture, are taken from the literature ($G_N^0 = 160$ kPa, $\tau_e = 0.007$ s, $M_e = 18$ kg/mol [26]) and confirmed by the rheological measurements of the Pristine sample.

The output of the code is the MMD of the different strands and the weight fractions of different chain segments as mentioned above: segments without stickers (called "linear chains"), segments belonging to a chain with only one sticker (each of the arms is called "star-like strand"), and segments trapped between two stickers (called "trapped strands between two stickers") or located at the chain extremity (called "dangling ends"). The number- and weight-average molar masses of the components are defined from the model considering a Flory distribution (polydispersity of 2). In particular, the number-average mass of a trapped segment is estimated to be m_{unit}/p; hence, its weight-average molar mass is $2m_{\text{unit}}/p$. The latter is strictly related to the plateau region discussed below.

For a large average molar mass between two associated units, the probability to have loops, hence possible intrachain associations, is neglected when compared to the more probable interchain associations. The proportions of the different components are then used to predict the $G(t)$ and extract G' and G''.

In the case of reversible bonds, in addition to the probability p_1 that a monomer is a reversible sticker, a second parameter, τ_{sticker}, which is the average lifetime of the bond, is considered. Similarly to the sticky reptation model [41], the stickers are treated as friction points and the lifetime of the bonds as the extra friction felt by the chain because of the association/disassociation dynamics. Here, the friction is equally distributed over the entire chain, introducing a delay of the relaxation of the network, as described in the Appendix. To this end, an additional term in the expression of the characteristic times (reptation and early fluctuation) is considered, following the approach of [22,27].

Finally, the moduli of the double networks are calculated based on the hypothesis that the polymer network at long times comprises permanent stickers only and includes linear chains, dangling strands, and trapped stands; the reversible stickers are able to associate/dissociate with a characteristic time. In other words, at times longer than the lifetime of the reversible bonds, the network is considered to be permanent, with the reversible bonds acting as extra friction elements along the network strands (delaying their relaxation). Furthermore, we assume that the segments trapped between two permanent crosslinkers never relax, neglecting the possibility of H-like structures with long backbones able to relax at very long times. The probability of observing this relaxation is effectively negligible due to the small density of crosslinkers and the presence of very long dangling ends.

Also for this network, the parameters used to describe the dynamics are τ_{sticker} and p (p_1 and p_2). Note that the predictions for the double networks consider the same value of τ_{sticker} used for the reversible single networks since they are characterized by the same reversible bonds.

Analyzing the dynamics of double networks with one permanent component and considering that the density of entanglements is larger than the density of crosslinkers, we can identify distinct regimes from high to low frequencies (see also Fig. 1),

I. At very high frequencies, local Rouse relaxation takes place, corresponding to the local reorientation of the entanglement segments.

II. A rubbery plateau appears next, as the frequency decreases, due to both the entanglements and the associated units, which prevent the chains from further relaxing. The corresponding value of the plateau modulus is

$$G_N^0 = \frac{c\,\rho_{\text{melt}} RT}{M_{e,XX}}, \tag{2}$$

with c being the dilution factor accounting for the presence of the short chains that behave as solvent and $M_{e,XX}$ being the average molar mass between two entanglements or crosslinkers,

$$\frac{1}{M_{e,XX}} = \frac{1}{M_e} + \frac{1}{M_{XX}}. \tag{3}$$

The average molar mass between two associated units, M_{XX}, is determined from p_1 and p_2 and the molar mass of a chain unit, m_{unit} (152 g/mol),

$$M_{XX} = \frac{2m_{\text{unit}}}{p_1 + p_2}. \tag{4}$$

This plateau extends up to the frequency marking the relaxation of free chains, star-like segments, and dangling ends, which can disentangle without requiring the dissociation of the reversible stickers. This partial disentanglement of the chains also induces the partial disentanglement of the trapped segments by CR process.

III. Then, a second plateau appears, due to the chain segments trapped between two crosslinkers, which are unable to relax and disentangle,

$$G_{N,1}^0 = \upsilon_{\text{trapped}}^2 \frac{c\,\rho_{\text{melt}} RT}{M_{e,XX}}, \tag{5}$$

with $\upsilon_{\text{trapped}}$ being the weight fraction of polymer segments trapped between two crosslinking points (reversible or permanent) [26].

If all crosslinkers are permanent, no further relaxation mechanism is observed and the plateau remains at low frequencies.

IV. If the sample contains reversible bonds, the polymer is able to further relax at frequencies below the inverse lifetime of these transient junctions. Only the molecular segments between two permanent bonds cannot relax fully, but only partially through a sticky Rouse process. As

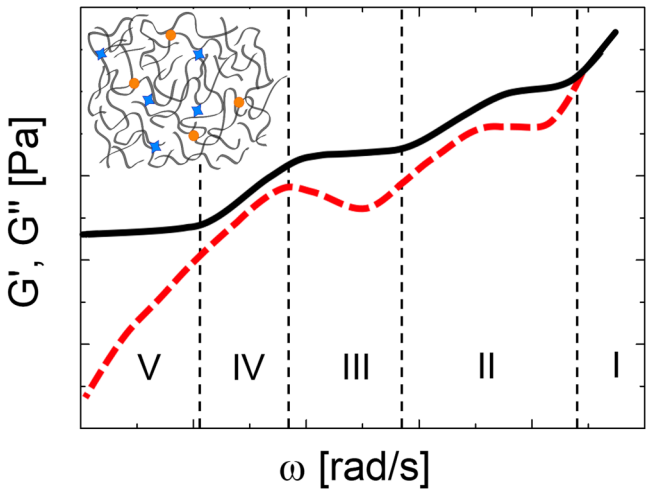

FIG. 1. Graphical illustration of the linear viscoelastic response of double networks with one permanent component, divided into the five different regimes described from the model (see text). G' corresponds to the black solid line and G'' to the red dashed line. Cartoon: double network of gray polymeric chains with two types of bonds, permanent (orange circles) and reversible (blue stars).

detailed in the Appendix, in this regime, the model considers the reversible stickers as extra friction points rather than extra branching points.

V. Then, a third (low-frequency) rubbery plateau develops, which reflects the effective entanglements trapped between two permanent bonds (stickers), $(c\,\rho_{\mathrm{melt}}RT)/M_{e,XX,2}$,

$$G^0_{N,2} = \upsilon^2_{\mathrm{trapped,\,2}}\,\frac{c\,\rho_{\mathrm{melt}}RT}{M_{e,XX,2}}, \tag{6}$$

where $\upsilon_{\mathrm{trapped,2}}$ is the weight fraction of polymer segments between two permanent crosslinking points and $M_{e,XX,2}$ is the average molar mass between two entanglements or permanent bonds. The latter is determined as

$$M_{XX,2} = \frac{2m_{\mathrm{unit}}}{p_2}. \tag{7}$$

Therefore, the term $\upsilon^2_{\mathrm{trapped,\,2}}$ accounts for all dangling ends not trapped between two permanent stickers (which we effectively "remove") and their CR effect.

III. RESULTS AND DISCUSSION

A. Experimental results

The linear viscoelastic master curves of the different networks are reported in Fig. 2. The data reveal the influence of the different nature of stickers on the relaxation of the network. Due to the large polydispersity, the Pristine sample exhibits a very broad peak of G'' (almost smeared out), and the complete terminal relaxation of the system (with $G' \sim \omega^2$ and $G'' \sim \omega^1$) has not been reached in the experimentally accessible frequency window, even if the terminal moduli crossover is detected [see Fig. 2(a)]. For the same reason, the different regimes discussed in Sec. II cannot be clearly discerned. The introduction of reversible bonds [see Fig. 2(b)] delays the relaxation processes and, consequently, the terminal crossover is shifted to lower frequency; the trapped chains can, indeed, renew their configuration only when the junctions have exchanged partners. Regarding the network formed from permanent crosslinks [see Fig. 2(c)], the dynamics are distinctly different. The trapped strands between bonds inhibit the network relaxation and a low-frequency plateau regime is anticipated (corresponding to regime V in Fig. 1). Actually, for Permanent I, the second plateau is not observed, even with creep measurements, due to the small fraction of permanent crosslinks and the respective dominant fraction of free linear chains and dangling ends able to relax and act as an effective solvent for the network. By increasing the fraction of bonds (Permanent II), the fraction of trapped strands increases and a plateau is clearly observed at lower frequencies [$G^0_{N,2}$, see Eq. (6)]. Permanent II exhibits also a minimum in G'' at lower frequencies [10^{-6} rad/s in Fig. 2(c)], which has been detected with creep measurements. To validate the obtained results, we report in Fig. S3 of the supplementary material [48] the creep compliance at different values of the applied stress. The low-frequency behavior could be attributed to the relaxation of internal inhomogeneities (for example, long segments or clusters formed in the network that take longer time to relax) or to the possible presence of branching generation of segments, moving slowly but still able to relax, similarly to the inner segments of a Cayley tree [42]. The double networks behave similarly to the permanent networks [see Fig. 2(d)]. In particular, no low-frequency plateau or double peak of G'' is observed in the experimentally accessible time window because of the small fraction of crosslinkers. This is further highlighted by the results of creep and recovery tests (see Fig. S4 in the supplementary material [48]), which show that a time-independent value of creep compliance and respective complete strain recovery is only reached for sample Permanent II with a larger fraction of bonds (see also low-frequency plateau in the frequency spectra of Fig. 2).

Overall, when comparing the response of all networks (see Fig. S5 in the supplementary material [48]), they exhibit identical local dynamics (expectedly since the polymers have the same chemistry), and the level of their first plateau modulus is similar. This is consistent with the fact that it mainly depends on the density of entanglements since the samples contain a few stickers only. Hence, the examined networks meet the Dalqhuist criteria and, consequently, a good contact with surfaces is ensured. The nature and density of the crosslinks can alter the terminal relaxation of the networks and, therefore, affect their ability to resist detaching forces. They also affect their long-time behavior.

B. Analysis of the data with the TMA model

In Fig. 3, the predictions from the TMA model are compared against the experimental data. The model is able to describe satisfactorily the viscoelastic spectra of the networks over a broad range of frequencies. Importantly, it predicts the long-time viscoelastic response of the networks, which was

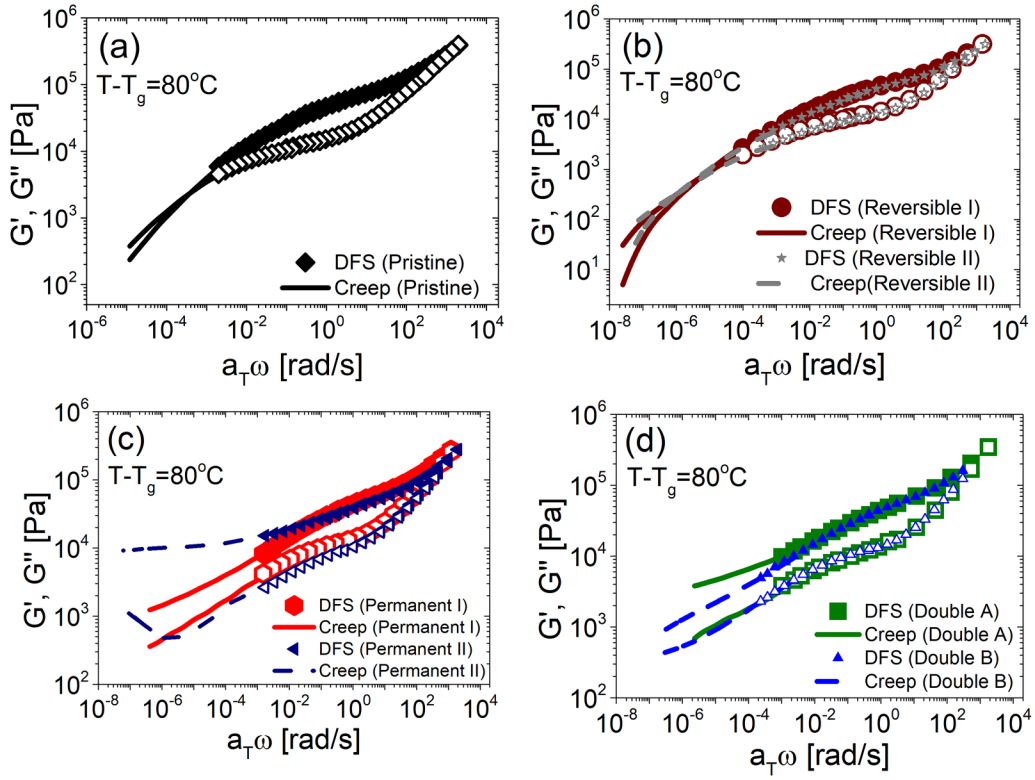

FIG. 2. Linear viscoelastic master curves of the networks with different crosslinkers, representing G' (solid symbols) and G'' (open symbols) as a function of the shifted oscillatory frequency. In (a) we report with black diamonds the data obtained for Pristine, in (b) for Reversible I (wine red circles) and Reversible II (gray stars), in (c) for Permanent I (red hexagons) and Permanent II (navy blue left triangles), and in (d) the behavior of Double A (green squares) and Double B (blue up triangles). The data are reported at the same distance from T_g. In each plot, symbols correspond to the results obtained by DFS and lines (dashed and solid) by creep.

not accessible experimentally. However, it does not capture the increase of G'' at low frequencies observed with sample Permanent II since it does not consider possible inhomogeneities in the networks and the relaxation of an inner generation of segments.

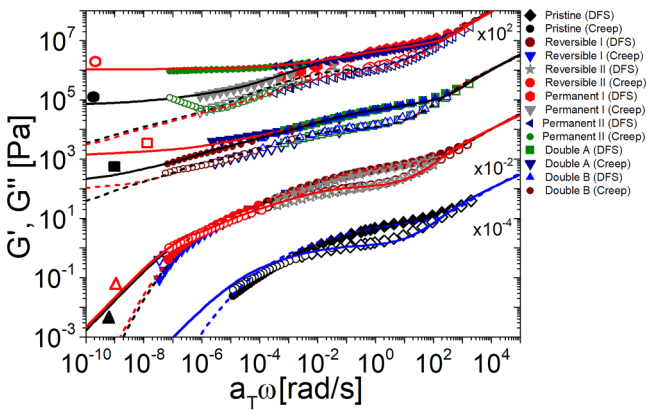

FIG. 3. Linear viscoelastic moduli as a function of the shifted frequency: experimental data are symbols (solid symbols for G', open symbols for G''; data extracted from DFS or creep are reported in the legend) and model predictions are lines (solid lines for G', short-dashed lines for G''). The data have been shifted vertically (by factors indicated on the plot) for clarity. Blue lines are used for Pristine sample; black lines for Reversible I, Permanent I, and Double B; and red lines for Reversible II, Permanent II, and Double A. Black lines are indicated by black solid triangle (Reversible I), solid circle (Permanent I), and solid square (Double B); red lines by red open triangle (Reversible II), open circle (Permanent II), and open square (Double A).

As already explained, the agreement between model predictions and experimental data was achieved by determining the "best-fit" values of the association probabilities of the chain units (p_1 for reversible bonds and p_2 for permanent bonds) and for the sticker lifetime, τ_{sticker}, of the reversible bonds. The same value of τ_{sticker} (350 s) was used for both the reversible and the double networks. The corresponding molecular characteristics were estimated from p_1 and p_2, accounting for the weight fractions of the different species of molecular segment and the molar masses between two reversible stickers (abbreviated as rev), two associated stickers M_{XX}, or between two permanent stickers (abbreviated as perm) $M_{XX,2}$, based on Eqs. (4) and (7). The values of the different parameters used are reported in Table III.

It can be evidenced from Table III that the networks are characterized by a significant presence of linear chains and dangling ends. As shown in Fig. 4 (and Fig. S6 in the supplementary material [48]), the short chains are mainly uncrosslinked, while the trapped segments are only observed for the chains with the largest molar mass (MM), and account in general for less than 10% of the entire chain population. Furthermore, analysis of the distribution of segments reveals that combining reversible and permanent crosslinks in the double network A allows to have trapped segments of smaller MM, which can be detected from a slight shift of the distribution of trapped segments toward lower values of MM, compared to the corresponding permanent network (see Fig. S6(a) in the supplementary material [48]). As evidenced

TABLE III. Modeling parameters and derived quantities for the investigated networks: values of p_1, p_2, and MM between stickers and total amount of the different segments constituting the networks.

Network	p_1	p_2	MM between stickers $\times 10^{-6}$ (g/mol)	Linear chains (wt. %)	Star chains (wt. %)	Dangling ends (wt. %)	Trapped strands (wt. %)
Reversible I	1/10 000		1.5	68.81	18.36	7.09	5.74
Reversible II	1/8000		1.2	66.15	18.25	8.35	7.25
Permanent I		1/7500	1.14	64.52	18.92	8.44	8.12
Permanent II		1/2000	0.225	34.8	18.4	15.7	31.1
Double A	1/5000	1/6770 1.02 (perm) 0.435 (M_{xx})	0.76 (rev)	46.2 (perm)	15.4 (perm)	18 (perm)	20.4 (perm)
Double B	1/9000	1/10 500	1.37 (rev) 1.6 (perm) 0.74 (M_{xx})	71.5 (perm)	16.25 (perm)	6.8 (perm)	5.45 (perm)

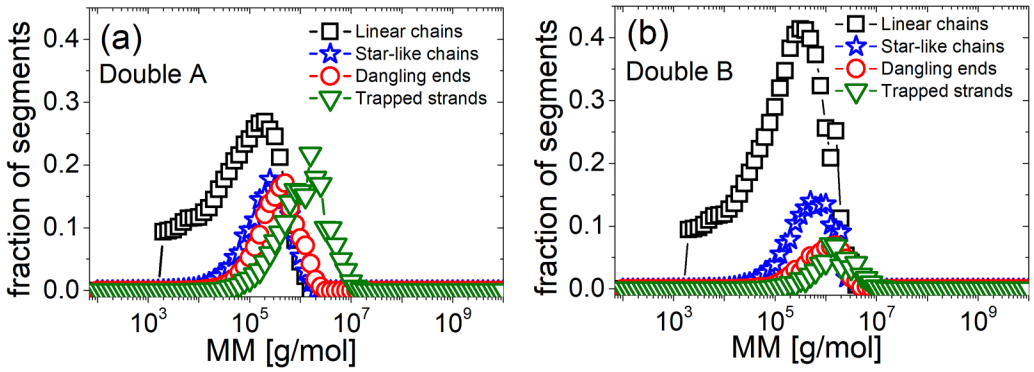

FIG. 4. Distribution of the molar mass (MM) of the different segments, obtained for Double A (a) and Double B (b) from the model. Black open squares represent the distribution of linear chains, blue open stars of star-like chains, red open circles of dangling ends, and green open down triangles of trapped segments, localized between the two end-associating units. The possible segments formed are based on both reversible and covalent bonds.

from Fig. 4(a), the peak intensity of the trapped segments is similar to the one of dangling ends and star-like chains (possible differences observed are considered to be minor), indicating a comparable concentration of these categories of segments. A decrease in the peak intensity of the trapped segments along with an increase in the linear chain peak is depicted comparing Double B with Double A and demonstrates an increase in linear chains at the expense of trapped segments. The analysis of the sample composition and the low proportion of effectively active permanent bonds ($M_{xx,2} = 1020$ and 1600 kg/mol for Double A and Double B, respectively, compared to $M_e = 18$ kg/mol) explains why the terminal regime and the low-frequency plateau are reached at very long times, highlighting that the networks are not or weakly percolated, which is a common feature for PSAs (and thought to ensure the balance between viscous and elastic solid behavior).

The best-fit values of p were determined by considering first the highest probability $p_{\max}$ of a monomer to be a crosslinking point (Table IV), estimated from the network's chemical composition and expressed as

$$p_{\max} = \frac{\text{Number of crosslinkers}}{\text{Number of chains}} = \frac{\text{Mol of crosslinkers}}{\text{Mol of chains}}. \quad (8)$$

These values were chosen in order to accurately describe the experimental data, keeping in mind that values higher than $p_{\max}$ would not be reasonable, implying the presence of more crosslinkers than the real amount estimated from chemistry. Comparing the two probabilities, extracted from the chemical composition and best-fit analysis, the proportion of bonds that are uncrosslinked and do not contribute to the viscoelasticity of the networks can be determined (Table IV). The presence of a small fraction of unreacted crosslinker can be attributed to the industrial-scale production of the investigated materials or to the reactivity of the bonds (since in the

TABLE IV. Parameters used in the analysis of the networks. Values of MM between stickers and $p_{\max}$ estimated from the weight fraction of stickers and unreacted crosslinkers.

Network	*MM* between stickers $\times 10^{-5}$ (g/mol)	$p_{1,\max}$	$p_{2,\max}$	Unreacted crosslinkers (wt. %)
Reversible I	4.3	1/2900		71
Reversible II	3.03	1/2000		75
Permanent I	1.02		1/6770	9
Permanent II	3.03		1/2000	0
Double A	4.3 (rev) 1.02 (perm) 3.03 (M_{xx})	1/2900	1/6770	42 (rev) 0 (perm)
Double B	6.5 (rev) 1.4 (perm) 4.5 (M_{xx})	1/4300	1/9500	50 (rev) 9 (perm)

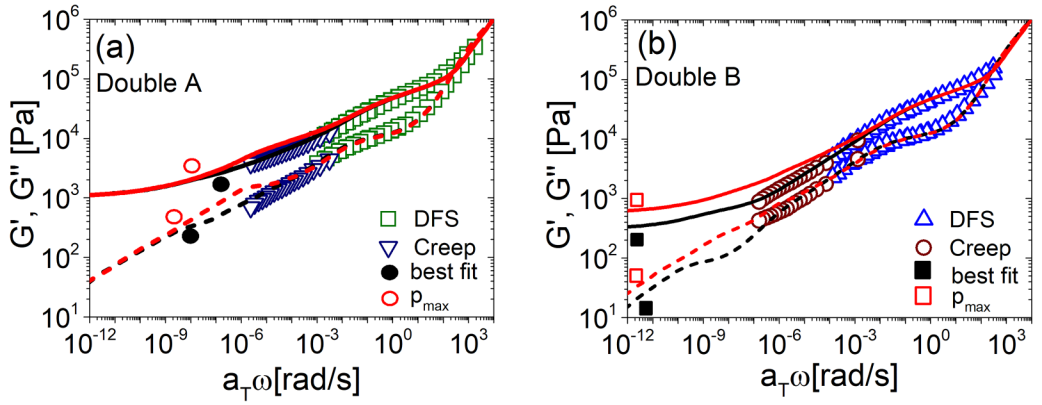

FIG. 5. Comparison of the experimental data with predictions obtained considering the best-fit values for p, as reported in Table III (black solid line for G', black short-dashed line for G'') and p_{max} (G' with red solid line, G'' with red short-dashed line), for the two networks. (a) Double A (DFS data are reported with green open squares and creep data with navy blue open down triangles), (b) Double B (DFS data with blue open up triangles, creep data with wine red open circles). Symbols are also reported to identify the different lines (the predictions). The predictions obtained with: p_{max} are marked with open red circles (a) and open red squares (b); best-fit values with solid black circles (a) and solid black squares (b).

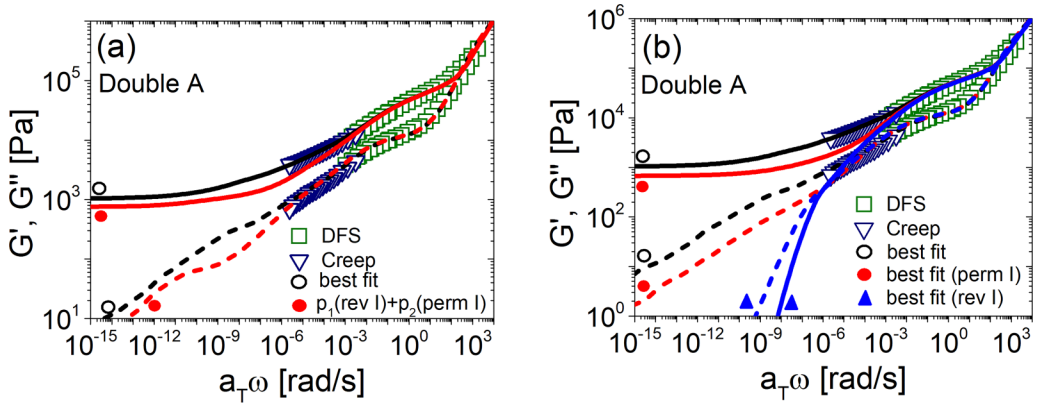

FIG. 6. (a) Experimental data of Double A [green open squares (DFS) and navy blue open down triangles (creep)] and predictions obtained using the best-fit values of the double network ($p_1 = 1/5000$ and $p_2 = 1/6770$) (black lines, and marked by black open circles at the end of the lines) and the respective values of Reversible I and Permanent I ($p_1 = 1/10\,000$ and $p_2 = 1/7500$, with red lines and marked by red solid circles). (b) Comparison of the best fit obtained for Double A (black lines and black open circles at the end), Reversible I (blue lines and blue solid triangles at the end of the lines), and Permanent I (red lines and red solid circles at the end of the lines). In both figures, G' is reported with solid lines and G'' with short-dashed lines.

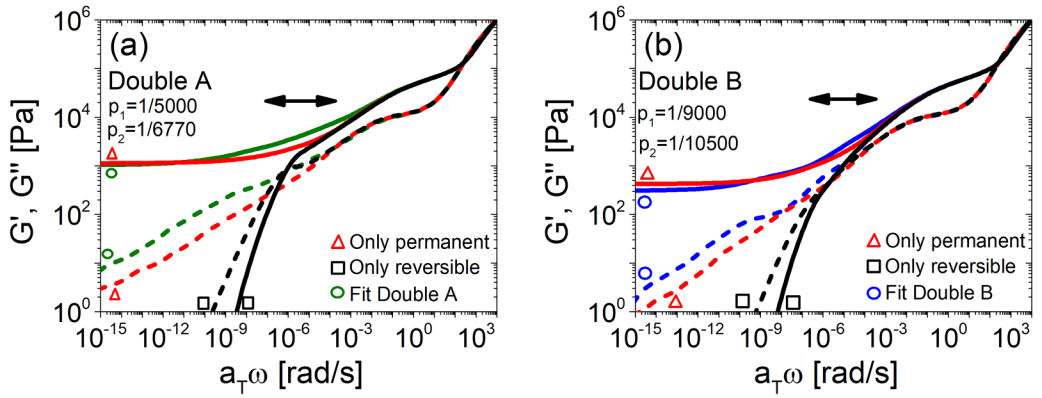

FIG. 7. Predictions of the moduli of Double A (a) and Double B (b) [green and blue lines, respectively, and marked with green (a) and blue (b) open circles] compared with the prediction of the respective networks bonded by only physical (black lines and indicated by black open squares) and only chemical cross-links (red lines and indicated by red open triangles) and considering the same values of p used in the model for an optimum fit of the data [$p_1 = 1/5000$ (a) and $p_1 = 1/9000$ (b) for the single reversible networks, $p_2 = 1/6770$ (a) and $p_2 = 1/10\,500$ (b) for the single permanent networks]. G' is reported with solid lines and G'' with short-dashed lines. The arrows indicate the intermediate regime which is mainly affected by the presence of reversible bonds.

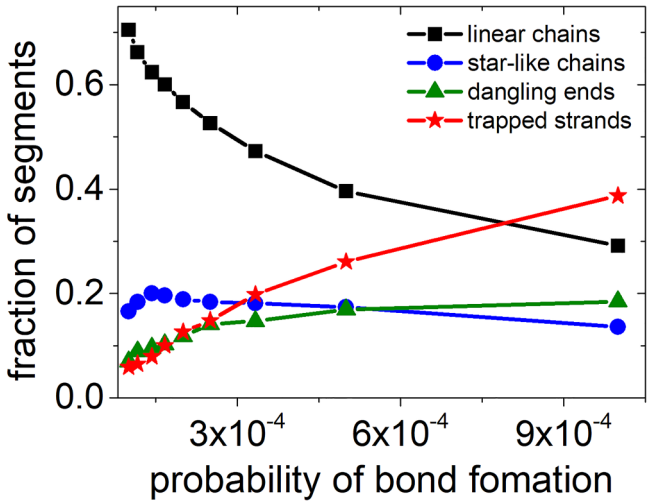

FIG. 8. Effect of the relative number of stickers (expressed as probability of bond formation) on the relative amount of the different types of polymeric strands (again, expressed as probability). The increase in bonding probability leads to the reduction of linear chains in favor of trapped strands.

case of reversible networks the fraction of unreacted bonds is higher).

In Fig. 5, the model predictions obtained with p_{max} are compared to the predictions obtained with best-fit value of p for the double networks. Small deviations are observed, which are attributed to the possible presence of unreacted crosslinkers in the systems. Additional analysis with fitting individual components data (Permanent I, Reversible I, II) is presented in Fig. S7 of the supplementary material [48].

As the relative fraction of reversible/permanent stickers in Double A corresponds to the respective fractions in Reversible I and Permanent I, the contribution of the different dynamical (reversible) stickers to the viscoelastic response of Double A was predicted by using the fitting parameters already obtained from the single networks analysis (hence, using $p_1 = 1/10\,000$ and $p_2 = 1/7500$). The obtained prediction for Double A, plotted as the red curves in Fig. 6, does not match the experimental data. In particular, deviations are observed mainly at intermediate frequencies, where the dynamics are affected by the reversible stickers. By decreasing the distance between reversible bonds (i.e., increasing p_1), it is possible to obtain a better description of the data, suggesting a smaller amount of unreacted bonds in the double network. This reduction can be justified by topological effects and the corresponding likelihood that the constraints coming from the permanent network increase the probability of the reversible stickers to bond and, hence, contribute to the viscoelasticity of the networks.

Furthermore, in Fig. 6(b), the very similar behavior of the double and permanent networks highlights the fact that the experimentally investigated double networks are mainly affected by the presence of the permanent bonds. The reversible bonds slightly influence the viscoelastic spectra at intermediate frequencies. This can also be understood by looking at Fig. 7, where we assess the contribution of the different crosslinkers by considering the predictions obtained with the best-fit values of p_1 and p_2 (Table III). This figure depicts the role of each crosslinker type independently, considering the same value of p_1 and p_2 used for the description of the experimental data of the double network. In both cases, the linear viscoelastic behavior of the present double network resembles that of the network with only permanent bonds, apparently because of the lower amount of reversible bonds. However, slight deviations are observed in the intermediate-frequency regime (indicated by arrows in Fig. 7), where the reversible stickers slow down the constraint release Rouse (CRR) events, hence delaying the appearance of the second plateau. From this comparison, we can conclude that adding reversible stickers to a permanent network allows to tailor the intermediate-frequency response of the PSA double network. Additional analysis results examining the contributions of components Permanent II and Reversible II to Double A are depicted in Fig. S8 of the supplementary material [48]. In fact, by using the combination of $p_1 = 1/4000$, $p_2 = 1/12\,000$ and $\tau_{sticker} = 50\,000$ s, it is possible to obtain double network features resembling the response reported in Fig. 1 (see Fig. S9 in the supplementary material [48]).

C. Effects of p and $\tau_{sticker}$

Using the model, it is illuminating to explore the roles of sticker lifetime and density of stickers on the linear

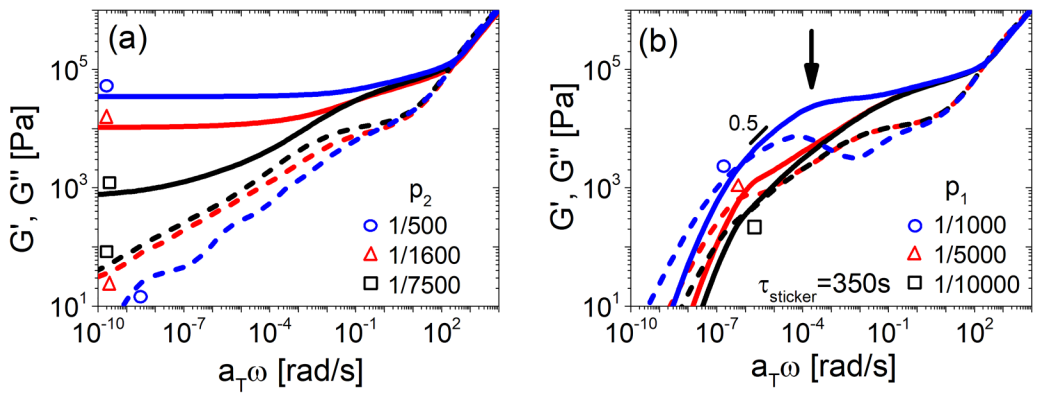

FIG. 9. Storage and loss moduli predicted with different density of permanent (a) and reversible stickers (b), in the last case $\tau_{sticker}$ is equal to 350 s. The predictions are reported with black lines and marked with black open squares [$p_2 = 1/7500$ (a), $p_1 = 1/10\,000$ (b)], red lines and marked with red open triangles [$p_2 = 1/600$ (a), $p_1 = 1/5000$ (b)], and blue lines and blue open circles [$p_2 = 1/500$ (a), $p_1 = 1/1000$ (b)]. The arrow in (b) indicates the low-frequency mode and the short line with slope 0.5 the Rouse scaling (see the text). G' is represented with solid lines and G'' with short-dashed lines.

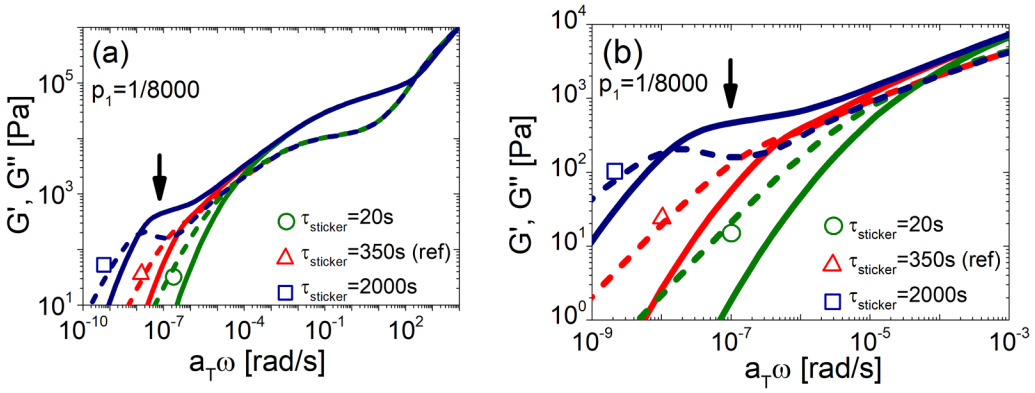

FIG. 10. (a) Linear viscoelastic spectra of reversible networks predicted by considering a constant value of p_1 (1/8000) and different lifetime of stickers: $\tau_{sticker} = 20$ s (green lines and green open circle at the end of G''), $\tau_{sticker} = 350$ s (redlines and red open triangles at the end of G''), $\tau_{sticker} = 2000$s (navy blue lines and navy blue open squares at the end of G''). (b) Magnification on the low-frequency region of the data reported in (a), showing the time evolution of the slow mode and plateau. Solid lines represent G' and short-dashed lines G''. The arrows indicate the low-frequency mode (see the text).

viscoelastic response of the networks. Therefore, in the following figures, the predictions of the model are presented by varying these parameters for single and double networks. The effect of the density of stickers can be investigated by changing the value of p as an input parameter of the model and estimating the fraction of the different types of segments. In particular, as shown in Fig. 8, by increasing p, the fraction of linear chains (without stickers) decreases, while the fractions of trapped segments and dangling ends increase, leaving almost constant the amount of star-like chains. This translates into different viscoelastic behavior, depending on the fraction of reversible bonds as well. In the case of double network, the respective amounts estimated are based on permanent stickers and represent the composition of the networks at a long time, when reversible stickers are already relaxed.

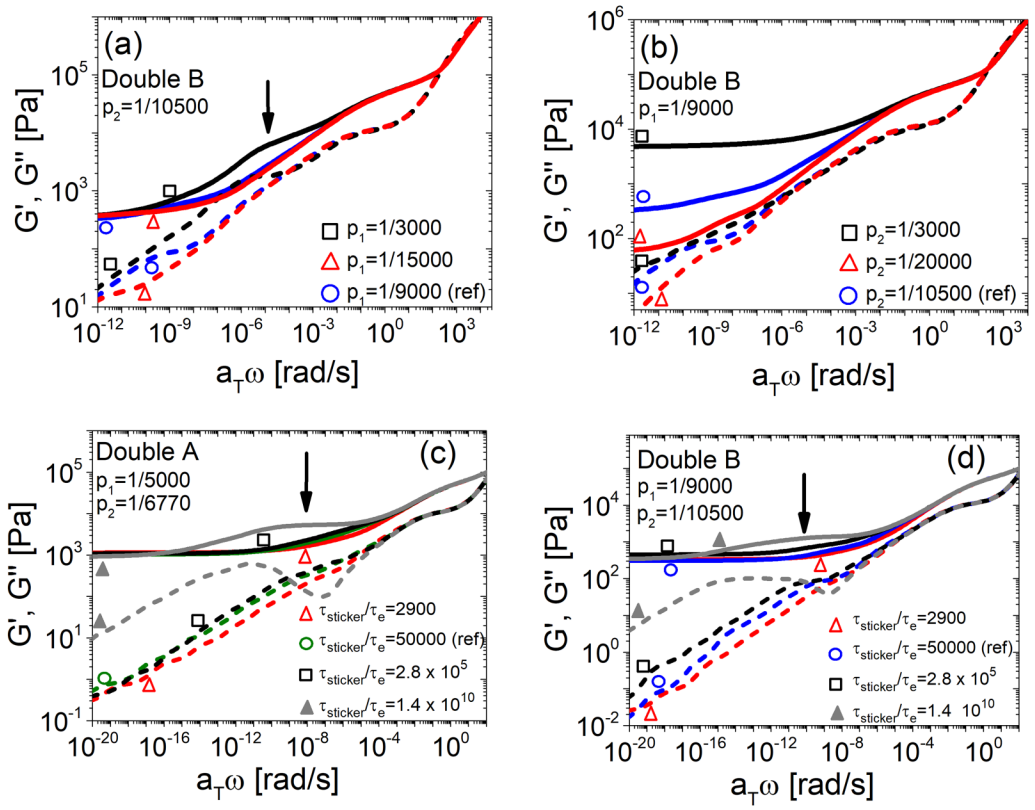

FIG. 11. Storage and loss moduli predicted considering different amounts of crosslinkers for network Double B with fixed $\tau_{sticker}$, with p_1 varied and p_2 constant (a), or the opposite (b). Predictions with different lifetime of the reversible sticker are reported for the networks Double A (c) and Double B (d) without changing the values of p_1 and p_2 used to validate the model. The frequency regime above 100 rad/s is not reported for clarity of presentation, focusing here on the more interesting lower-frequency regime. The predictions corresponding to the experimental networks studied in this work are reported with blue lines and marked with blue open circles in (a) and (b), with green (c) and blue (d) lines and marked with green and blue open circles in (c) and (d), respectively. The arrows indicate the intermediate mode (see the text).

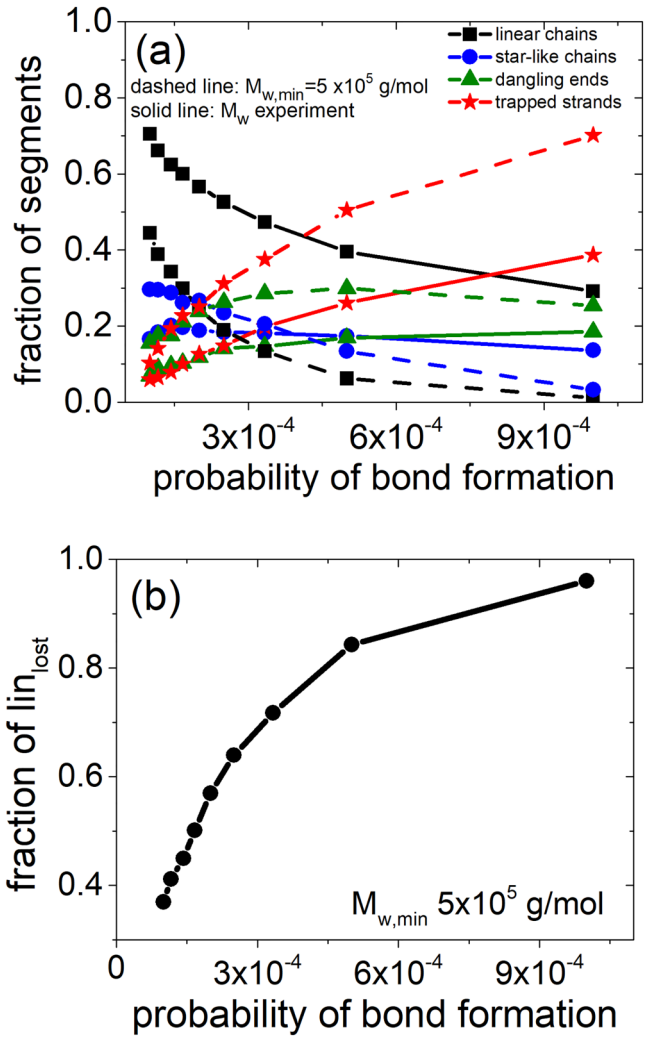

FIG. 12. (a) Proportion of the segments as a function of the relative number of stickers obtained considering the MMD provided (solid lines) and the case without chains having MM below 5×10^5 g/mol (dashed lines). In both cases, linear chains are reported with square symbols, star-like chains with circles, dangling ends with up triangles, and trapped segments with stars. (b) Respective fraction of linear chains lost when small chains are removed (due to the change in $M_{w,\min}$).

As shown in Fig. 9, for the case of permanent bonds, increasing the permanent crosslinking density, p_2, will raise the level of the low-frequency plateau in G' because of smaller $M_{xx,2}$ and respective larger weight fraction of trapped strands which are not going to relax at longer times. On the other hand, if the bonds are reversible, the predictions reveal a second slow peak of G'' due to the delayed relaxation of the physically crosslinked segments, which becomes significant with an increasing amount of stickers. Nevertheless, the terminal flow starts at a similar time (identified at the moduli crossover) since the lifetime of the stickers is the same. Since the molar mass between stickers is larger than the one between entanglements, the dynamics linked to disentanglements and disassociation of the stickers are distinct. This is evidenced by the appearance of two distinct modes, with plateau or broadening in the G' curve and two peaks in the G'' curve (see also Fig. 10). The low-frequency mode (affected also by the lifetime of stickers) is more visible in the case of $p_1 = 1/1000$, where the G' value [marked by arrows in Figs. 9(b) and 10] is only slightly lower than the high-frequency plateau G_N^0 [see Eq. (2)]. The second mode is followed by the Rouse relaxation of the sticky chains as depicted by the 0.5 slope of G' with frequency. Only when the stickers disassociate, the strands between crosslinks can relax by Rouse-like terminal motion.

The situation involving segments between crosslinkers shorter than those between entanglements (higher values of p) has not been investigated because it is outside the scope of the present work, which focuses on networks with density of entanglements larger than the crosslinking density, relevant for PSAs. Consequently, in Fig. 9, the presence of stickers influences the dynamics at intermediate and low frequencies without altering the higher-frequency plateau-G' region.

To examine the influence of the sticker lifetime, we then fix the value of p to that used for Reversible II network ($p_1 = 1/8000$) and change the value of τ_{sticker}. The introduction of stronger bonds into the reversible networks, implemented by the larger value of τ_{sticker} (Fig. 10), yields slower dynamics and a clear second plateau appears for long τ_{sticker} (2000 s), due to trapped segments that can relax only after the disassociation of the reversible bonds. The transition regime between the two modes (or plateau values) corresponds to the relaxation of the free and dangling molecular segments, followed by the partial disentanglement of the trapped segments by the CRR process. Hence, it is possible to change the lifetime of the bonds to accommodate the long-time properties needed in a particular application.

Building-up on the above results, the model was further used to explore the dynamics of a double network by considering different fractions of bonds and different lifetimes of the reversible stickers. The results are summarized in Fig. 11. We observe that the increase of p_1 (with p_2 being kept constant) leads to a second slow peak of G'' at intermediate frequencies, which reflects the relaxation of segments bonded with reversible stickers and a related weak plateau of G' [arrow in Fig. 11(a)] corresponding to regimes III and IV of Fig. 1. The networks are formed by a larger fraction of trapped segments with smaller $M_{xx,2}$, which are unable to completely relax and disentangle before the bonds disassociate, and contribute to the intermediate plateau. On the other hand, increasing p_2 (with p_1 being kept constant) mainly affects the low-frequency permanent plateau of G' due to the increased fraction of trapped segments in the double networks (see also Fig. 9). It must be further noted that changes in the viscoelasticity with τ_{sticker} are observed when the lifetime of bonds is significantly increased; this is observed in Figs. 11(c) and 11(d), where we report the effect of the latter parameter in relation to τ_e which was extracted from the data. For the lower values of the ratio $\tau_{\text{sticker}}/\tau_e$ considered (2900, 5000, and 2.8×10^5), the lifetime of the bonds does not affect the dynamics, as the friction related to the stickers is negligible compared to the friction coming from the backbone that mainly affects the chain diffusion. In this case, the addition of reversible bonds alters the viscoelastic behavior [see arrows in Figs. 11(c) and 11(d)] slightly, however, may significantly affect the nonlinear rheological properties when

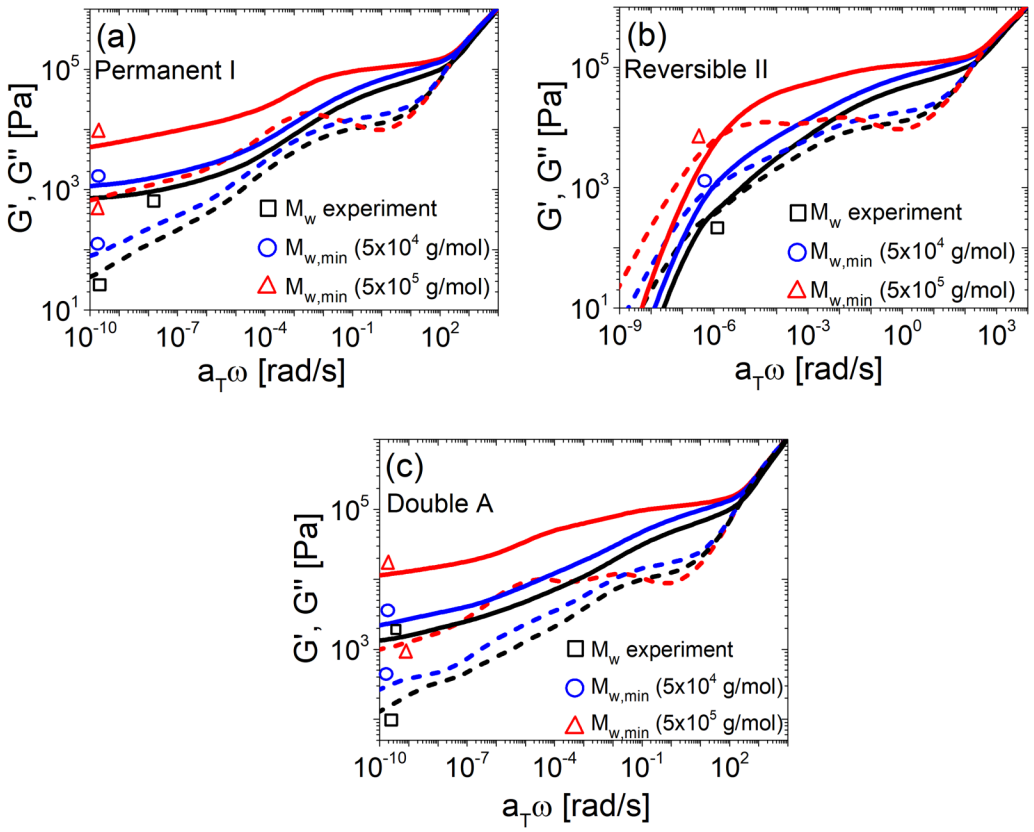

FIG. 13. Predicted linear viscoelastic spectrum of the double network when reducing the amount of smaller chains, thus considering different $M_{w,\min}$ (5×10^5 g/mol in red lines and 5×10^4 g/mol in blue lines, the first are indicated by red open triangles and the second by blue open circles) of the molar mass distribution provided (black lines and indicated by black open squares). G' is reported with solid lines and G' with short-dashed lines. The predictions are reported for Permanent I (a), Reversible II (b), and Double A (c).

large deformations (at rates larger than $1/\tau_{\text{sticker}}$) are imposed on the material, which are relevant to adhesion performance [43–46]. This will be the subject of future investigations. When $\tau_{\text{sticker}}/\tau_e$ is equal to 1.4×10^{10} (gray lines in Fig. 11), a second, low-frequency plateau in G' appears, as in regimes III and IV, because the stickers behave as effective permanent bonds. As observed by the appearance of regimes III and IV in Fig. 11, by changing the values of the model parameters, it is possible to define the conditions necessary to observe the typical feature of double networks and to tune the properties of the systems accordingly to their application.

D. Effects of MMD

To elucidate the effects of low-MM components in the polydisperse network, the reported MMD (Appendix, Fig. 14) was considered, however with the smallest chains being removed, thus changing its minimum MM, $M_{w,\min}$. Specifically, in Fig. 12, we present the effects of removing the smaller chains ($M < 5 \times 10^5$ g/mol) on the fraction of polymer segments, which correspond to the reduction of 37% of the total number of chains (value obtained from the MM distribution as done for the estimation of c). In particular, the same total weight fraction of chains was considered to keep a constant value of the dilution (corresponding to $c = 86\%$).

It is observed that the network that does not contain the smallest chains is characterized by a lower fraction of free chains, rapidly evolving toward zero when the probability of association increases. The fraction of linear chains "lost" (due to the change of $M_{w,\min}$) as a function of the bonding probability is reported in Fig. 12(b). Furthermore, in this case, the network contains a larger fraction of trapped segments, becoming mechanically stronger, as observed in Fig. 13.

In fact, for all networks investigated, a significant increase in the trapped segments and consequently of the sample elasticity is observed when a fraction of the smallest chains are absent. Furthermore, in the case of reversible networks, accounting or not for these small chains does not substantially alter the terminal relaxation time, since the latter is linked to the disassociation time and density of the bonds, which remain practically unchanged with or without the small chains. Furthermore, eliminating the small chains from network Double A leads to the appearance of a clear second peak of G'' at lower frequencies. Hence, the removal of low-MM fractions is associated with the formation of more elastic networks, which exhibit stronger resistance to external forces and, expectedly, lower tackiness [3,47].

IV. CONCLUSIONS AND PERSPECTIVES

The linear viscoelastic properties of a set of industrial PSAs were investigated by combining shear oscillatory and creep rheometry with an appropriately modified tube-based TMA model which accounts for the network's dynamic

composition. Comparing model predictions and experimental data, we showed that TMA can be extended to inhomogeneous (not well-controlled synthesis conditions) and polydisperse polymeric materials, such as the present industrial polymers, and predict their complex linear dynamics. It is possible that the present networks also comprise clusters or branched chains, which are not currently considered in the model. Accounting for them with appropriate modifications would help in reducing the small deviations between experimental data and model predictions and should be addressed in future studies.

Our results demonstrate the crucial role of the nature of the bonds in dictating the long-time behavior of the double networks, without altering the short-time response, which is only linked to the presence of entanglements. Reversible crosslinkers delay the relaxation process because the segments formed can only relax after the bonds change partners (disassociate and reassociate). On the other hand, when permanent bonds are introduced to the network, a second plateau appears at low frequencies, reflecting the small fraction of trapped segments. The linear viscoelastic response of double networks is primarily influenced by the presence of permanent bonds, with reversible stickers slightly affecting the intermediate-frequency regime. The model allowed examining the influence of changing p_1, p_2, $\tau_{sticker}$, and MMD on the structural composition of the double networks and consequently their viscoelasticity spectra. Hence, it may be used for improving the design of such materials for targeted applications and extended to entangled networks with different polymer compositions or MMD, having a small amount of stickers with different dynamic behavior.

These results set the stage for future nonlinear rheological studies. For example, it will be interesting to consider the time of imposed deformation in comparison to the lifetime of the reversible stickers, as we expect that when deforming the networks faster than $1/\tau_{sticker}$ the reversible bonds shall behave as permanent stickers and the samples may become brittle [44–46].

ACKNOWLEDGMENTS

The financial support from the European Union's Horizon 2020 Programme for Research and Innovation under the Marie Skłodowska-Curie Grant Agreement No. 765811 (DoDyNet) is gratefully acknowledged. E.v.R. is a Research Associate of the FRS-FNRS.

APPENDIX: CHARACTERIZATION AND MODELING DETAILS

1. Molecular characterization by MMD

The predictions obtained with the model were realized using the MMD provided by TESA SE and considering 14% of the short polymer chains acting as a solvent. This is justified by the peak analysis of the experimental MMD reported in Fig. 14, and by estimating the ratio between the two areas. In particular, we consider that chains with MM below 10^3 g/mol act as a solvent. Consequently, the MMD used in the model does not include the distribution of the blue circle area.

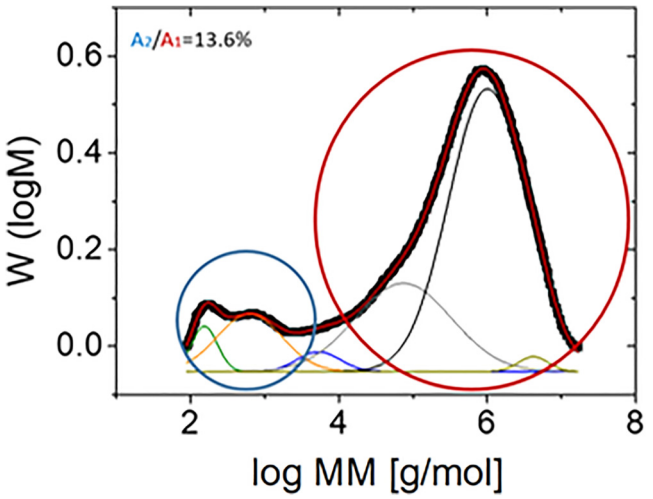

FIG. 14. Peak analysis of the experimental MMD. The blue circle identifies the area of MM considered solvent in the systems. The horizontal axis reports the logarithm of the molar mass.

2. Modified TMA

The typical relaxation mechanisms involved are described following the approach in [32]. The relaxation of the different segments formed by the stickers is described considering the basic relaxation mechanisms, but additionally including extra delays in the reptation and fluctuation processes due to the extra friction introduced by the reversible stickers. In fact, because of the presence of stickers along the chains these processes can only occur when the bonds are disassociated and segments are able to move and disentangle.

In the case of contour length fluctuations, which is the only way for the formed dangling ends and arms of star-like chains (defined based on the permanent bonds, i.e., on p_2) to relax completely, the extra friction coming from the reversible stickers is taken into account only for the early fluctuation mechanisms, assuming negligible influence on the activated fluctuation. It is described similarly to the extra friction coming from the branches of a comb [23] or a pom-pom polymers [28]. More specifically, while with a branched molecule, the extra friction per branch is determined by considering that a branching point takes a time equal to the relaxation time of the branch to cover the distance between two entanglements, the extra friction per sticky group is determined by considering that a sticky chain takes a time equal to $\tau_{sticker}$ to diffuse the same distance. Therefore, the total friction felt by the chains is expressed as in Eq. (A1), which includes the contribution of the monomeric friction (the first term) and the extra friction from the sticky points (the second term). Using the same concept as for the relaxation of comb polymers, the latter is related to the number $q_{sticker}$ and lifetime $\tau_{sticker}$ of the stickers,

$$\xi_{tot} = \xi_0 N + \frac{2q_{sticker}\tau_{sticker}kT}{a^2}, \tag{A1}$$

where N is the number of monomers, ξ_0 is the monomeric friction independent of the stickers, and a is chosen to be the

size of an entanglement segment (keeping analogy to branched polymers).

Consequently, an additional term reflecting the number and lifetime of stickers was thus included in the early fluctuations term, in order to account from this extra friction coming from the q_{stickers} stickers along the chain backbone,

$$\tau_{\text{early}}(x) = \frac{9\pi^3}{16}\left(\frac{\left(\frac{M}{2}\right)}{M_e}\right)^2 \tau_{\text{Rouse}}\, x^4\, c^2 + \frac{3\pi}{8} q_{\text{stickers}} \left(\frac{\left(\frac{M}{2}\right)}{M_e}\right)^3 \tau_{\text{sticker}}\, x^4\, c^3, \tag{A2}$$

where τ_{Rouse} is the Rouse lifetime, M_e is the molar mass between the entanglements, M is the molar mass of the chain, x is the fractional distance which is equal to 0 at the free ends of the chain and to 1 in the middle, c is the dilution factor for the presence of short chains behaving as solvent. The delay time, which is equi-distributed along the entire chain, is determined by considering that the trapped entanglements can move and fluctuate only after the disassociation of the stickers.

The characteristic diffusion of a segment i along the tube and, therefore, the probability of its relaxation by reptation is described, at time t and position x, by the classic Doi–Edwards equation

$$p_{\text{rep}}(x_i, t) = \sum_{p\ \text{odd}} \frac{4}{p\pi} \sin\left(\frac{p\pi x_i}{2}\right) \exp\left(\frac{-p^2 t}{\tau_{\text{rept}}}\right), \tag{A3}$$

where τ_{rept} is the reptation time considering the contribution coming from the friction of the chain itself [the first term in Eq. (A3)] and the extra friction due to the reversible stickers [the second term in Eq. (A3)]. The chains and the entanglements trapped between stickers can indeed reptate only when the stickers disassociate allowing the entanglements (Z) to relax and move, carrying extra friction due to the stickers,

$$\tau_{\text{rept}} = 3\tau_e Z^3\, c + \frac{2 q_{\text{stickers}}\, \tau_{\text{sticker}}}{\pi^2} Z^2\, c^2. \tag{A4}$$

As in previous works [28,29], a chain relaxes by reptation when its center of mass has diffused a distance L_{eq}, the equilibrium tube length. The model considers a small time-scale separation between reptation and fluctuation processes; consequently, the relaxed segments were not considered extra solvent for the unrelaxed ones.

REFERENCES

[1] Creton, C., "Pressure-Sensitive adhesives: An introductory course," MRS Bull. **28**, 434–439 (2003).

[2] Benedek, I., and M. M. Feldstein, *Fundamentals of Pressure Sensitivity* (CRC, Boca Raton, 2009).

[3] Crosby, A. J., and K. R. Shull, "Adhesive failure analysis of pressure-sensitive adhesives," J. Polym. Sci., Part B: Polym. Phys. **37**, 3455–3472 (1999).

[4] Benedek, I., *Pressure-Sensitive Adhesives and Applications* (CRC, New York, 2004).

[5] Daristotle, J. L., S. T. Zaki, L. W. Lau, O. B. Ayyub, M. Djouini, P. Srinivasan, M. Erdi, A. D. Sandler, and P. Kofinas, "Pressure-Sensitive tissue adhesion and biodegradation of viscoelastic polymer blends," ACS Appl. Mater. Interfaces **12**, 16050–16057 (2020).

[6] Czech, Z., and R. Kurzawa, "Acrylic pressure-sensitive adhesive for transdermal drug delivery systems," J. Appl. Polym. Sci. **106**, 2398–2404 (2007).

[7] Chen, X., Y. Wang, Z. Cheng, J. Wei, Y. Shi, and J. Qian, "Diffusion behavior of drug molecules in acrylic pressure-sensitive adhesive," ACS Omega **5**, 9408–9419 (2002).

[8] Musazzi, U. M., M. A. Ortenzi, C. G. M. Gennari, A. Casiraghi, P. Minghetti, and F. Cilurzo, "Design of pressure-sensitive adhesive suitable for the preparation of transdermal patches by hot-melt printing," Int. J. Pharm. **586**, 119607–119615 (2020).

[9] Marin, G., and C. Derail, "Rheology and adherence of pressure-sensitive adhesives," J. Adhes. **82**, 469–485 (2006).

[10] Kaelble, D. H., "Peel adhesion: Influence of surface energies and adhesive rheology," J. Adhes. **1**, 102–123 (1969).

[11] Callies, X., O. Herscher, C. Fonteneau, A. Robert, S. Pensec, L. Bouteiller, G. Ducouret, and C. Creton, "Combined effect of chain extension and supramolecular interactions on rheological and adhesive properties of acrylic pressure-sensitive adhesives," ACS Appl. Mater. Interfaces **8**, 33307–33315 (2016).

[12] Dahlquist, C. A., "Pressure sensitive adhesives," in *Treatise on Adhesion and Adhesives*, edited by R. L. Patrick (Marcel Dekker, New York, 1969), Vol. 2.

[13] da Silva, L. F. M., A. Ochsner, and R. D. Adams, *Handbook of Adhesion Technology* (Springer, Berlin, 2011).

[14] Brown, K., J. C. Hooker, and C. Creton, "Micromechanisms of tack of soft adhesives based on styrenic block copolymers," Macromol. Mater. Eng. **287**, 163–179 (2002).

[15] Arrington, K. J., S. C. Radzinski, K. J. Drummey, T. E. Long, and J. B. Matson, "Reversibly cross-linkable bottlebrush polymers as pressure-sensitive adhesives," ACS Appl. Mater. Interfaces **10**, 26662–26668 (2018).

[16] Courtois, J., I. Baroudi, N. Nouvel, E. Degrandi, S. Pensec, G. Ducouret, C. Chanéac, L. Bouteiller, and C. Creton, "Supramolecular soft adhesive materials," Adv. Funct. Mater. **20**, 1803–1811 (2010).

[17] Li, X., Y. Deng, J. Lai, G. Zhao, and S. Dong, "Tough, long-term, water-resistant, and underwater adhesion of low-molecular-weight supramolecular adhesives," J. Am. Chem. Soc. **142**, 5371–5379 (2020).

[18] Heinzmann, C., C. Weder, and L. M. de Espinosa, "Supramolecular polymer adhesives: Advanced materials inspired by nature," Chem. Soc. Rev. **45**, 342–358 (2016).

[19] Kim, E. S., D. B. Song, K. H. Choi, J. H. Lee, D. H. Suh, and W. J. Choi, "Robust and recoverable dual cross-linking networks in pressure-sensitive adhesives," J. Polym. Sci. **58**, 3358–3369 (2020).

[20] Dobson, A. L., N. J. Bongiardina, and C. N. Bowman, "Combined dynamic network and filler interface approach for improved adhesion and toughness in pressure-sensitive adhesives," ACS Appl. Polym. Mater. **2**, 1053–1060 (2020).

[21] Mayumi, K., A. Marcellan, G. Ducouret, C. Creton, and T. Narita, "Stress–strain relationship of highly stretchable dual cross-link gels:

Separability of strain and time effect," ACS Macro Lett. **2**, 1065–1068 (2013).

[22] Cao, L., J. Huang, and Y. Chen, "Dual cross-linked epoxidized natural rubber reinforced by tunicate cellulose nanocrystals with improved strength and extensibility," ACS Sustainable Chem. Eng. **6**, 14802–14811 (2018).

[23] Gong, J. P., Y. Katsuyama, T. Kurokawa, and Y. Osada, "Double-network hydrogels with extremely high mechanical strength," Adv. Mater. **15**, 1155–1158 (2003).

[24] Ducrot, E., Y. Chen, M. Bulters, R. P. Sijbesma, and C. Creton, "Toughening elastomers with sacrificial bonds and watching them break," Science **344**, 186–189 (2014).

[25] Honerkamp, J., and J. Weese, "A nonlinear regularization method for the calculation of relaxation spectra," Rheol. Acta **32**, 65–73 (1993).

[26] Weese, J., "A regularization method for nonlinear ill-posed problems," Comput. Phys. Commun. **77**, 429–440 (1993).

[27] Van Gurp, M., and J. Palmen, "Time-temperature superposition for polymeric blends," Rheol. Bull. **67**, 5–8 (1998).

[28] van Ruymbeke, E., C. Bailly, R. Keunings, and D. Vlassopoulos, "A general methodology to predict the linear rheology of branched polymers," Macromolecules **39**, 6248–6259 (2006).

[29] Ahmadi, M., C. Bailly, R. Keunings, M. Nekoomanesh, H. Arabi, and E. van Ruymbeke, "Time marching algorithm for predicting the linear rheology of monodisperse comb polymer melts," Macromolecules **44**, 647–659 (2011).

[30] Lentzakis, H., S. Costanzo, D. Vlassopoulos, R. H. Colby, D. J. Read, H. Lee, T. Chang, and E. van Ruymbeke, "Constraint release mechanisms for H-polymers moving in linear matrices of varying molar masses," Macromolecules **52**, 3010–3028 (2019).

[31] Ahmadi, M., A. Jangizehi, E. van Ruymbeke, and S. Seiffert, "Deconvolution of the effects of binary associations and collective assemblies on the rheological properties of entangled side-chain supramolecular polymer networks," Macromolecules **52**, 5255–5267 (2019).

[32] Hawke, L. G. D., M. Ahmadi, H. Goldansaz, and E. van Ruymbeke, "Viscoelastic properties of linear associating poly(n-butyl acrylate) chains," J. Rheol. **60**, 297–310 (2016).

[33] Ahmadi, M., L. G. D. Hawke, H. Goldansaz, and E. van Ruymbeke, "Dynamics of entangled linear supramolecular chains with sticky side groups: Influence of hindered fluctuations," Macromolecules **48**, 7300–7310 (2015).

[34] Zhuge, F., L. G. D. Hawke, C. A. Fustin, J. F. Gohy, and E. van Ruymbeke, "Decoding the linear viscoelastic properties of model telechelic metallo-supramolecular polymers," J. Rheol. **61**, 1245–1262 (2017).

[35] de Gennes, P. G., "Reptation of a polymer chain in the presence of fixed obstacles," J. Chem. Phys. **55**, 572–579 (1971).

[36] Doi, M., and S. F. Edwards, *The Theory of Polymer Dynamics* (Clarendon, Oxford, 1986).

[37] Doi, M., W. W. Graessley, E. Helfand, and D. S. Pearson, "Dynamics of polymers in polydisperse melts," Macromolecules **20**, 1900–1906 (1987).

[38] van Ruymbeke, E., R. Keunings, and C. Bailly, "Prediction of linear viscoelastic properties for polydisperse mixtures of entangled star and linear polymers: Modified tube-based model and comparison with experimental results," J. Non-Newtonian Fluid Mech. **128**, 7–22 (2005).

[39] Schwarzl, F. R., "Numerical calculation of storage and loss modulus from stress relaxation data for linear viscoelastic materials," Rheol. Acta **10**, 165–173 (1971).

[40] Likhtman, A. E., and T. C. B. McLeish, "Quantitative theory for linear dynamics of linear entangled polymers," Macromolecules **35**, 6332–6343 (2002).

[41] Leibler, L., M. Rubinstein, and R. H. Colby, "Dynamics of reversible networks," Macromolecules **24**, 4701–4707 (1991).

[42] van Ruymbeke, E., K. Orfanou, M. Kapnistos, H. Iatrou, M. Pitsikalis, N. Hadjichristidis, D. J. Lohse, and D. Vlassopoulos, "Entangled dendritic polymers and beyond: Rheology of symmetric Cayley-tree polymers and macromolecular self-assemblies," Macromolecules **40**, 5941–5952 (2007).

[43] Lamanna, G., and A. Basile, "Mechanics of soft PSAs (pressure sensitive adhesives)," Open Mater. Sci. J. **7**, 23–28 (2013).

[44] Shabbir, A., Q. Huang, Q. Chen, R. H. Colby, N. J. Alvarez, and O. Hassager, "Brittle fracture in associative polymers: The case of ionomer melts," Soft Matter **12**, 7606–7612 (2016).

[45] Shabbir, A., Q. Huang, G. P. Baeza, D. Vlassopoulos, Q. Chen, R. H. Colby, N. J. Alvarez, and O. Hassager, "Nonlinear shear and uniaxial extensional rheology of polyether-ester-sulfonate copolymer ionomer melts," J. Rheol. **61**, 1279–1289 (2017).

[46] Yang, H., S. Wu, and Q. Chen, "How to choose a secondary interaction to improve stretchability of associative polymers?," Macromolecules **54**, 8112–8121 (2021).

[47] Lakrout, H., C. Creton, D. Ahn, and K. R. Shull, "Influence of molecular features on the tackiness of acrylic polymer melts," Macromolecules **34**, 7448–7458 (2001).

[48] See supplementary material at https://www.scitation.org/doi/suppl/10.1122/8.0000406 for details of rheometric data (Van Gurp–Palmen plots, shift factors, creep data, master curves, in Figs. S1–S5) and modeling analysis and predictions (molar mass distributions, comparison with experiments, predictions with different parameter values, in Figs. S6–S9).